Global aerosol optical models and lookup tables for the new MODIS aerosol retrieval over land

Robert C. Levy[1,2,3], Lorraine A. Remer[2] and Oleg Dubovik[4]

[1] Science Systems and Applications Inc., Lanham MD

[2] Laboratory for Atmospheres, NASA/Goddard Space Flight Center, Greenbelt MD

[3] Department of Atmospheric and Oceanic Science, University of Maryland, College Park, MD

[4] Lab. d'Optique Atmospherique, Univ. des Sciences et Tech. de Lille, Villeneuve d'Ascq, France

Corresponding author's address: Mr. Robert Levy
SSAI
Code 613.2
NASA/Goddard Space Flight Center
Greenbelt MD 20771
Email: levy@climate.gsfc.nasa.gov

301-614-6123 (voice)
301-614-6307 (fax)

Submitted for publication, JGR

July 2006

Global aerosol optical models and lookup tables for the new MODIS aerosol retrieval over land

Robert C. Levy, Lorraine A. Remer, Oleg Dubovik

Since 2000, MODIS has been deriving aerosol properties over land from MODIS observed spectral reflectance, by matching the observed reflectance with that simulated for selected aerosol optical models, aerosol loadings, wavelengths and geometrical conditions (that are contained in a lookup table or 'LUT'). Validation exercises have showed that MODIS tends to under-predict aerosol optical depth (τ) in cases of large τ (τ >1.0), signaling errors in the assumed aerosol optical properties. Using the climatology of almucantur retrievals from the hundreds of global AERONET sunphotometer sites, we found that three spherical-derived models (describing fine-sized dominated aerosol), and one spheroid-derived model (describing coarse-sized dominated aerosol, presumably dust) generally described the range of observed global aerosol properties. The fine-dominated models were separated mainly by their single scattering albedo (ω_0), ranging from non-absorbing aerosol (ω_0~0.95) in developed urban/industrial regions, to neutrally absorbing aerosol (ω_0~0.90) in forest fire burning and developing industrial regions, to absorbing aerosol (ω_0~0.85) in regions of savanna/grassland burning. We determined the dominant model type in each region and season, to create a 1° x 1° grid of assumed aerosol type. We used vector radiative transfer code to create a new LUT, simulating the four aerosol models, in four MODIS channels. Independent AERONET observations of spectral τ agree with the new models, indicating that the new models are suitable for use by the MODIS aerosol retrieval.

1. Introduction

One of the great scientific uncertainties is the role of aerosols within earth's climate system (IPCC, 2001). Aerosols are deeply involved in the radiation budget, cloud processes and air quality. Satellites are increasingly being used for observing global aerosol properties. Since MODIS' launch aboard *Terra* (in late 1999) and aboard *Aqua* (in early 2002), MODIS spectral reflectance observations have led to retrievals of aerosol optical depth (*AOD* or τ) and a measure of the aerosol size distribution, known as the fine model weighting (FW or η). Indeed, the most comprehensive aerosol dataset over land has been provided by MODIS (Remer et al., 2005), and such data has been used in dozens of applications and publications since launch. Not only have MODIS aerosol products been used to answer scientific questions about radiation and climate (e.g. IPCC, 2001; Yu et al., 2005), they are being used for applications such as monitoring surface air quality for health (e.g. Chu et al., 2003, Al-Saadi et al., 2005).

The recent operational version over land (V4.2) and the products created for Collection 004 (C004) were described in Remer et al., (2005). Even though the MODIS C004 aerosol products have been 'validated' by comparison with sunphotometer, they still show room for improvement, especially in certain environments. For example, Levy et al., (2005) determined that when compared to sunphotometer data, retrievals of AOD over the U.S. East Coast tended to over-predict τ in clean conditions, and under-predict in more hazy conditions. They postulated that the over-estimation in clean conditions was a result of poor land surface reflectance assumptions, and that the under-estimation of high τ was related to poor assumptions of aerosol optical properties. In a companion paper, Levy et al., (2006) discuss surface reflectance assumptions and introduce a new retrieval philosophy from MODIS. In this paper, we concentrate on improving the aerosol model assumptions.

The upward spectral 'reflectance' (normalized solar radiance) observed by a satellite at the top of the atmosphere (TOA) is a function of successive orders of radiation interactions within the coupled surface-atmosphere system. The observed spectral

reflectance results a combination of processes, including: scattering of radiation within the atmosphere without interaction with the surface (known as the 'atmospheric path reflectance'), the reflection of radiation off the surface that is directly transmitted to the TOA (the 'surface function'), and the reflection of radiation from outside the sensor's field of view (the 'environment function'). The environment function is neglected so that to a good approximation, the angular (function of solar zenith, sensor zenith and sun/sensor relative azimuth) TOA reflectance at a wavelength λ is described by:

$$\rho_\lambda^*(\theta_0,\theta,\phi) = \rho_\lambda^a(\theta_0,\theta,\phi) + \frac{F_\lambda(\theta_0)T_\lambda(\theta)\rho_\lambda^s(\theta_0,\theta,\phi)}{1 - s_\lambda\rho_\lambda^s(\theta_0,\theta,\phi)} \qquad (1)$$

where $F_{d\lambda}$ is the 'normalized downward flux' for zero surface reflectance, T_λ represents 'upward total transmission' into the satellite field of view, s_λ is the 'atmospheric backscattering ratio', and $\rho^s{}_\lambda$ is the angular 'surface reflectance'. Except for the surface reflectance, each term on the right hand side of Equation 1 is a function of the aerosol type (chemical composition, size distribution) and its columnar loading (τ).

The MODIS algorithm follows a lookup table (LUT) strategy, thereby assuming that a small set of aerosol types, loadings, and geometry can span the range of global aerosol conditions. The LUT contains pre-computed simulations of the non-surface terms in equation 1, for the assumed set of aerosol and geometrical conditions. The goal of the algorithm is to match the lookup table with the MODIS-observed spectral reflectance $\rho^m{}_\lambda$, to retrieve the associated aerosol properties (including τ and η). The difficulty lies in making the most appropriate assumptions about both the surface and atmospheric contributions.

As explained by Remer et al., (2005), the MODIS algorithm over land chooses from a set of fine-dominated aerosol models and a single coarse-dominated aerosol model. The selection of which fine-dominated aerosol model is fixed based on season and location. The coarse-dominated model (dust) is considered fixed, globally. For earlier versions (before V4.2) of the retrieval algorithm had a choice of two fine models (Kaufman et al., 1997), the 'urban/industrial', and the 'biomass burning/developing world', differing as to their refractive indices, single scattering albedos and phase functions. Each of these aerosol models was actually comprised of two or more lognormal modes (Kaufman et al., 1997), with their optical properties based on a

combination of laboratory studies and sunphotometer data (e.g. Remer et al., 1998). Ichoku et al., (2003) found that neither of the two fine models was sufficient to simulate the highly absorbing smoke seen over southern Africa. As a result, a third fine model ('highly absorbing') was added for use in Africa and other absorbing aerosol regions (Remer et al., 2005). For C004, the addition of the new 'highly absorbing' model improved the MODIS/sunphotometer comparison in southern Africa. Although never implemented into C004, Levy et al., (2005) showed that revising the urban/industrial model could help improve retrievals of high τ. It is expected, then, that retrievals in other regions (and global) would be improved by re-evaluating the aerosol optical models for MODIS.

Chapter 2 summarizes the new aerosol algorithm. Chapter 3 describes the AERONET data used to develop the new models. Chapter 4 discusses cluster analysis of the AERONET data. Chapter 5 fixes the aerosol type at given locations as a function of season. Chapter 6 introduces the radiative transfer and calculations for the new lookup tables.

2. The C005 aerosol retrieval algorithm

Levy et al., (2006) introduced a new aerosol algorithm (known as Version 5.2 or 'V5.2') for deriving aerosol properties from MODIS over land, intended for Collection 5 (C005). This new algorithm over land uses gas-absorption-corrected reflectance data in four spectral channels (0.47, 0.66, 1.24, and 2.12 μm; MODIS channels 3, 1, 5 and 7), retrieve total spectral 'aerosol optical depth' (AOD or τ) and 'Fine aerosol Weighting' (FW or η), reported at 0.55 μm, and 'surface reflectance' at 2.12 μm. In contrast to the previous family of algorithms (for C004 – Remer et al., 2005), 'V5.2' does not need to assume that aerosol is transparent in the 2.12 μm (i.e. surface reflectance = observed reflectance at 2.12 μm). Also, it is not necessary to assume that the surface reflectance values, in the two visible channels (0.47 and 0.66 μm), are fixed ratios of that at 2.12 μm.

Instead, 'V5.2' assumes that the relationship between the visible and 2.12 μm is a function of scattering angle and a Vegetation Index based on the 1.24 and 2.12 μm

observations. This means that the algorithm has some sensitivity to the type of angular and surface type effects seen by investigators such as Gatebe et al. (2001) and Remer et al. (2001). Using the assumed surface reflectance relationship, the algorithm inverts three of the channels (0.47, 0.66 and 2.12 μm) to retrieve the three pieces of information (τ, η and surface reflectance).

Like all previous versions of the over-land algorithm, as well as the MODIS over ocean algorithm (Remer et al., 2005; Tanre et al., 1997), the new algorithm is based on the lookup table (LUT) strategy. This means that the MODIS observations are compared with simulations made by radiative transfer (RT) code, for a small set of aerosol and angular conditions that 'represent' the possible array of global scenarios. The purpose of this paper, then, is to describe the aerosol optical models and RT that leads to the new LUT that is used in for deriving C005 products.

3. The AERONET L2A dataset

The sunphotometers of the Aerosol Robotic NETwork (AERONET- Holben et al., 1998) provide a comprehensive data set of aerosol properties. Operating at hundreds of sites globally, AERONET has been reporting at some sites since 1993 (http://climate.gsfc.nasa.gov). 'Sun' products are retrievals of spectral τ at four or more wavelengths (0.44, 0.67, 0.87 and 1.02 μm – some instruments provide more) resulting from observations of the spectral extinction of the direct sunbeam. They are provided every 15 minutes during the daytime. 'Sky' products are hourly estimates of aerosol size distribution, phase function and absorption properties, derived from the observed scattered spectral radiance in the almucantur. The sky products are derived about once per hour, and assume spherical aerosol particles (Dubovik and King, 2000) and/or spheroid particles (Dubovik et al., 2002; Dubovik et al., 2006). Under either particle assumption, the fundamental derived parameters include spectral τ, spectral complex refractive index, the volume distribution as a function of 22 radius size bins (dV/dlnR), and fitting error to the radiance measurements. Additional parameters are then calculated that include Angstrom exponents, properties of two (fine and coarse mode) lognormal

aerosol distributions, spectral single scattering albedo (*SSA* or ω_0) and asymmetry parameter (g) of the lognormal modes. These data go through rigorous calibration and cloud screening processes, resulting in ground-truth estimates of a number of aerosol properties. These are known as Level 2 AERONET retrievals (in this paper we designate them as 'L2A').

4. Deriving new aerosol optical models

A number have studies (e.g. Chu et al., 2002, Remer et al., 2005, Levy et al., 2005) have demonstrated that MODIS/AERONET regression of τ over land results in slope less than one; meaning that MODIS tends to under-retrieve τ, especially as τ increases. Ichoku et al., (2003) found that an aerosol model with larger absorption (lower ω_0) was necessary to simulate smoke produced by savanna fires over southern Africa. This highly absorbing smoke model was later included for deriving C004. Over the east coast of the United States, Levy et al. (2005) showed MODIS could be improved by using the urban/industrial aerosol model derived over Goddard Space Flight Center (GSFC) from AERONET data (Dubovik et al., 2002). These studies, along with other anecdotal evidence, suggested that the set of aerosol models should be re-evaluated. Even though the current L2A dataset isn't truly "global," it is the most comprehensive ground based quality-assured dataset available.

Omar et al., (2005) performed a "cluster analysis" of AERONET data and found that six aerosol models (composed of desert dust, biomass burning, background/rural polluted continental, marine, and dirty pollution, respectively) are sufficient for representing the entire AERONET dataset. They vary mainly by their ω_0 and size distribution. Two models are representative of very clean conditions (marine and background/rural). One of the models (dust) is coarse-dominated model, analogous to the MODIS coarse dust model, and three are fine models having different ω_0 (biomass burning, polluted continental, and dirty pollution), that are analogous to the C004 set of fine models.

Because the MODIS over-land retrieval employs only three channels (and suffers from surface and other contaminations), it is not able to select among choices of fine aerosol model. Therefore, the algorithm must assign the fine aerosol model apriori of the

retrieval. Unfortunately, the Omar et al. study (2005) leaves us one step short of this goal, since a unique fine model was not found at every site. Therefore, for use in selecting site unique aerosol models, we engaged in a "subjective" cluster analysis that would yield us designated models at each site.

4.1. Subjective Cluster Analysis of AERONET data

For our subjective cluster analysis, we downloaded about 136,000 L2A almucantur retrievals that were processed as of February 2005. These encompassed both spherical and spheroid retrievals. We discriminated the retrievals by the minimum quality parameters suggested by the AERONET team, including: τ at 0.44 μm greater than 0.4, solar zenith angle greater than 45°, 21 symmetric left/right azimuth angles, and radiance retrieval error less than 4%. The resulting data set was comprised of 13,496 spherical retrievals and 5128 spheroid retrievals.

In order to differentiate between aerosol types, we separated the AERONET data set into ten discrete bins of τ. Each bin, then, was used separately to differentiate aerosol types. Presumably, this would help to identify expected 'dynamic' properties (function of AOD) of each aerosol type (e.g. Remer et al., (1998)). For clustering, we employed the cluster analysis routines provided with the IDL (Interactive Display Language) software version 6.1. Beginning with the entire data set (separately each bin of τ), we clustered with respect to a number of aerosol optical parameters. In contrast to Omar et al. (2005), we desired to pursue not necessarily the most statistically significant clustering, but rather to identify distinct models useful for MODIS. With the goal of fine model identification in mind, we decided on clustering with respect to only two optical parameters: SSA (ω_0) at 0.67 μm and the asymmetry parameter (ASYM or g) at 0.44 μm. Presumably ω_0 separates non-absorbing aerosols (such as urban/industrial pollution – (Remer et al., 1998; Dubovik et al., 2002)) from much more absorbing aerosols (such as savanna burning smoke – (e.g. Ichoku et al., 2003; Dubovik et al., 2002)), and g at 0.44 μm would help differentiate between the phase functions of different (mainly fine mode – size similar to wavelength) aerosols. In the spirit of the C004 aerosol map (Remer et al., 2005), we looked for three clusters that represented three fine aerosol models.

Assuming three clusters for the entire AERONET dataset led to two clusters with thousands of points each and one with only 11 points. Presuming the eleven-point cluster to contain only outliers, we removed these points from the dataset, and also from the appropriate τ bins. Because the outliers were removed, now the cluster routine would not have to reach so far to find a place for these points, and could be performed again. Re-clustering resulted in three clusters for each τ bin, each having a reasonable number of points. We assumed that we were allowed to number the clusters so that in each τ bin, one cluster represents the combination of highest ω_0 and highest g (a 'non-absorbing' aerosol model), one cluster represents the lowest ω_0 and lowest g (an 'absorbing' aerosol model), and the third represents the middle combination values (the 'neutral' aerosol model). As for the coarse aerosol model, we found that a single cluster described the spheroid-based almucantur inversions (Dubovik et al., 2006). Since the sites contributing to spheroid data were primarily those known to be in dust regions, we assumed that the spheroid model represented coarse-dominated (presumably dust) aerosol.

4.2. Aerosol models around the globe

Like the C004 algorithm, the C005 algorithm must decide which of the three fine-dominated aerosol type to assume for the retrieval. Remer et al., (2005) showed how each aerosol type was designated into regions, including places where little was known about the prevailing aerosol type. For example, C004 assumed that smoke from tree forest fires (both tropical and high latitude forest) had the same optical properties as eastern Europe, most of Asia, and other developing regions. How should assumed aerosol type be distributed for C005?

The first step is to determine the aerosol type that best represents each AERONET site. For each site, and for each season, we computed the percentage of the retrievals attributed to each cluster. Figure 1 (a-d) displays pie-plots at each site, as a function of season. To remove poor statistics, we show pie plots only at sites having at least 10 observations (per season) during the history of AERONET. Unfortunately, this removes the many sites that have few retrievals of $\tau > 0.4$. Green pie segments represent the non-absorbing $\omega_0 \sim 0.95$ model (presumably urban/industrial aerosol), blue segments are the neutral $\omega_0 \sim 0.90$ model (presumably generic, forest smoke and developing world aerosol),

and red segments designate the highly absorbing ω_0~0.85 model (presumably savanna/grassland smoke aerosol). At most sites and most seasons, the aerosol type is as expected. Non-absorbing aerosol (green) dominates the U.S. East Coast and far western Europe, whereas highly absorbing aerosol (red) dominates the savannas of South America and Africa. Most other sites are dominated by neutral aerosol (blue) or are a mix of all clusters.

There are some exceptions to expectation, however. Surprisingly, Southeast Asia seems to be primarily non-absorbing aerosols, as opposed to the absorbing aerosol assumed for C004. Recent studies (e.g. Eck et al., 2005) confirm that aerosol in urban areas in far Southeast Asia is primarily non-absorbing. A few sites in Western Europe have large fractions of absorbing aerosol, yet the reason is not known.

Keeping in mind our goal of dividing the world into plausible aerosol types, we decided that each site should have an assumed aerosol type attached to it. The Neutral aerosol model was set as the default, and would be changed only if clear dominance of one of the other two aerosol types was observed. If either the non-absorbing or the absorbing aerosol occupied more than 40% of the pie, and the other occupied less than 20%, then the site was designated as the dominant aerosol type. For example, GSFC (39°N,77°W) during the summer months (JJA), recorded 87% non-absorbing and 13% neutral, meaning it would be designated as non-absorbing.

Figure 2 (a-d) displays the designated aerosol types at each site. As in Fig. 1, green represents non-absorbing, blue represents neutral and red designates absorbing aerosol types. Most site designations seem reasonable and were expected from our experience. North America during the summer (JJA) is split between non-absorbing and neutral aerosol types, much the same way (approximately -100° longitude) as was prescribed for C004. Southern Africa during the winter season (DJF) is solidly designated as absorbing aerosol (e.g. Ichoku et al., 2003). Western Europe is evenly split between non-absorbing and neutral (except for two absorbing sites), meaning that a subjective decision is needed here. To follow the C004 lineage, we chose the non-absorbing aerosol model for Western Europe.

Figure 3 plots the final decision for designating aerosol types around the globe, as a function of season. Note that where possible the shapes correspond with the clustering.

At some regions, however, some subjectivity was needed to connect areas. For example, even though insufficient data exists for Africa north of the equator, the known surface types and seasonal cycles suggest that heavy absorbing aerosol would be produced during the biomass burning season. Red designates regions where the absorbing aerosol is chosen, whereas green represents non-absorbing aerosol. The neutral ($\omega_0 \sim 0.90$) model is assumed everywhere else. These images were mapped onto a 1° longitude x 1° latitude grid, such that a fine aerosol type is assumed for each grid point, globally. This global map approach, that is not hardwired into the processing code, will allow for easy alterations as new information becomes available.

Table 1 displays the optical properties and size distributions for the Continental model, the three spherical (neutral, absorbing and non-absorbing) fine models and the one spheroid (e.g. Dubovik et al., 2006) coarse aerosol (dust) models. Figure 4 shows the size distributions for the four AERONET-derived models. Note the dynamic nature (function of τ) of the size properties of the fine models, especially the non-absorbing model.

Figure 5 plots the spectral dependence of τ (Fig 5A) and phase function at 0.55 μm (Fig 5B) for each model having $\tau_{0.55} = 0.5$. Note that even though the three fine-dominated models have similar τ spectral dependence, their phase function differs somewhat. The coarse model (spheroid-dust) has much smaller spectral dependence than any of the fine-dominated models, and nearly flat phase function in the 90°-180° scattering angle range observable by MODIS.

Figure 6 compares the phase function of each of the new C005 models as compared to the analogous models from the C004 algorithm. Changes are minimal (especially for the 90°-180° scattering angle range) for the non-absorbing (urban) and absorbing (heavy smoke) aerosol types. A possibly significant change is seen in the neutral (generic/moderate smoke) phase function. The most obvious change is in the 'dust' models, due to assuming spheroids instead of spheres. The differences are primarily in the MODIS scattering angle ranges, which could have a significant effect within the aerosol retrieval.

5. Radiative transfer and new lookup tables

5.1. Channel center wavelengths and Rayleigh optical depths

The MODIS 0.47 μm blue band (channel 3) stretches between 0.459 and 0.479 μm (http://modis.gsfc.nasa.gov). The sea-level Rayleigh optical depth (*ROD* or τ_R) drops drastically over this channel, from about 0.203 at 0.459 μm to 0.170 at 0.479 μm (Bodhaine et al., 1999). The choice of 'center' wavelength to model and its associated ROD is crucial to obtaining unbiased aerosol retrieval. This is also an issue for the red 0.66 μm channel (channel 1: 0.620 - 0.670 μm), but since the RODs are only about one-quarter as in the blue, the decision is much less crucial. In C004, the assumed ROD was 0.186 for channel 3 and 0.048 for channel 1. The 6S RT code (Vermote et al., 1997) models the MODIS channel filter functions, and suggests that the ROD values should be more like 0.193 and 0.051, respectively for the two channels. The MODIS aerosol over ocean algorithm (Tanre et al., 1997, Ahmed et al., 1981) assumes the RODs for the channels as 0.195 and 0.052, respectively.

For C005, re-evaluation of the MODIS channel filter functions showed that central wavelengths for channels 3 and 1 are 0.466 and 0.644 μm respectively. According to Bodhaine et al. (1999), associated sea-level ROD values are 0.194 and 0.052, respectively, which leads to consistency with the aerosol over ocean algorithm. Similar calculations for the 0.55 and 2.12 μm channels (channels 4 and 7), found center wavelengths of 0.553 and 2.119 μm and RODs of 0.092 and 0.0004, respectively. Note that although the center wavelengths are known, we will continue to designate MODIS channels 3, 4, 1 and 7 as the 0.47, 0.55, 0.66 and 2.12 μm channels, for brevity and consistency with common usage. Table 2 lists the MODIS aerosol channels, along with the Rayleigh optical depth assumed for the band.

5.2. Radiative transfer code

The C004 (and previous) LUTs were calculated using 'SPD', the scalar version of the RT code written by Dave et al., (1970), a code that is a standard in the remote sensing community. However, Fraser et al (1989) suggested and Levy et al., (2004) demonstrated that under some geometries, neglecting polarization would lead to significant errors in top of atmosphere reflectance, further leading to significant errors (> 10% or > 0.1) in τ retrieval. Dave also provided a vector (polarized) option to the code (VPD), although it has not been well maintained within the MODIS community. Therefore, we need a vector code that is well understood and suitable for creating the LUT. In scalar mode, our choice of RT code should be consistent with the Dave benchmark. Also, it should reasonably match the Ahmed et al., (1981) calculations used for the over ocean aerosol retrieval (Remer et al., 2005).

Levy et al., (2004) employed RT3, the polarized radiative transfer model of Evans and Stephens (1991). This plane-parallel adding/doubling code allows for polarization to be turned on or off, by changing only one line within an input file. Thus, it was easy to compare the results to the Dave code's scalar mode, and then upgrade to vector mode to include polarization effects. Under most geometries and optical depths, differences between the two RT codes are less than 0.001 (which is about 1%).

As in Levy et al., (2004), the spherical aerosol scattering phase function elements (inputs to RT3) were calculated by integrating (over size distribution) the results of MIEV Mie code (Wiscombe et al., 1980) for hundreds of discrete radii. Properties of the aerosol size distribution and refractive indices were those described by Table 1. For the spheroids of the coarse aerosol model, Mie theory is not sufficient. We used instead, a version of the T-matrix code described in Dubovik et al., (2002, 2006), to calculate the scattering properties of the aerosol model. Not only is this a necessary approximation for integrating a spheroid size distribution, it is consistent with the calculations used in fitting the original almucantur radiance in the first place.

5.3. Description of the lookup table (LUT)

As introduced by Levy et al., (2006), the new V5.2 algorithm over land performs a simultaneous inversion of three channels (0.47, 0.66 and 2.12 μm) to retrieve τ, η and the surface reflectance. The inversion technique requires that the LUT be 'indexed' like for the over-ocean algorithm (Tanre et al., 1997; Remer et al., 2005). Since the principal product is τ at 0.55 μm, the LUT is indexed in relation to this channel.

Therefore, the C005 LUT is computed at the four central wavelengths (0.466, 0.553, 0.644 and 2.119 μm) representing the MODIS channels 3, 4, 1 and 7. The aerosol model-dependent parameters of equation 1 are calculated for several values of aerosol total loadings (indexed by τ at 0.55 μm), and for a variety of geometry. Each of the spherical aerosol models (Continental, neutral, absorbing and non-absorbing) and the one spheroid model (dust) are represented within the LUT.

The scattering/extinction efficiencies (Q_{sca} and Q_{ext}) of the aerosol size distributions are calculated by either MIEV or the Dubovik T-matrix code, depending on the assumed shape. Assuming a Rayleigh atmosphere and realistic layering of the aerosol, the Legendre moments of the combined Rayleigh/aerosol are computed for each layer of a US Standard Atmosphere (U.S. Government, 1976). These moments are fed into RT3 to simulate TOA reflectance and total fluxes.

The scattering and reflectance parameters are calculated for seven aerosol loadings ($\tau_{0.55}$ = 0.0, 0.25, 0.5, 1.0, 2.0 3.0, and 5.0). TOA reflectance is calculated for 9 solar zenith angles (θ_0 = 0.0, 6.0, 12.0, 24.0, 35.2, 48.0, 54.0, 60.0 and 66.0), 16 sensor zenith angles (θ = 0.0 to 66.0, increments of 6.0), and 16 relative azimuth angles (ϕ = 0.0 to 180.0 increments of 12.0). All of these parameters are calculated assuming a surface reflectance of zero.

When surface reflectance is present, the second term in Equation 1 is nonzero. The flux is a function only of the atmosphere, however, the atmospheric backscattering term, s, and the transmission term, T, are functions of both the atmosphere and the surface. Therefore, RT3 is run two additional times with distinct positive values of surface reflectance.

$$s = (1/\rho_1^s)(1-(F_d T \rho_1^s/(\rho^* - \rho^a)))$$

and (2)

$$s = (1/\rho_2^s)(1-(F_d T \rho_2^s/(\rho^* - \rho^a)))$$

Here, we chose values of 0.1 and 0.25 for our surface reflectance. ρ^s_1 and ρ^s_2. These two equations can be solved for the two unknowns, s and T. The values of F_d, s, and T are saved into the LUT, for each τ index, wavelength and aerosol model. The scattering and extinction coefficients, Q, are saved into the LUT. In addition, a parameter known as the Mass Concentration coefficient (M_c) is reported (see Appendix for its derivation).

6. Spectral dependence of aerosol models

How well do our derived models represent ambient aerosol at specific AERONET sites? For this purpose, we used the time series of Level 2 'sun' retrieved products from AERONET, which are independent of the 'sky' retrieved products. We cannot use the sun measurements to evaluate the assumed absorption properties, but we can analyze the spectral dependence of the aerosol optical depth.

The LUT is indexed by optical depth at 0.55 μm, in increments including τ = 0.25, 0.5, 1.0 and 2.0. Figure 5A showed the spectral τ dependence of each model for $\tau_{0.55}$=0.5. Similar plots could be made from the spectral dependence of the other indices within the LUT. For each AERONET site, we separated retrievals into three-month seasons (winter = DJF, spring = MAM, summer = JJA, fall = SON). Observations within each season were sorted according to $\tau_{0.55}$, where $\tau_{0.55}$ was calculated by fitting a quadratic to the observed spectral τ. For each indexed value of $\tau_{0.55}$ (τ = 0.25, 0.5, 1.0, 2.0), we determined which AERONET observation contained $\tau_{0.55}$ closest in magnitude to the indexed value. This we considered this location the 'central' (C_i) index of the bin. The total number of observations 'N_t' in each season, divided by 20, determined the number 'N' of observations that should be considered close to the 'central' index. Therefore, the set of AERONET observations for the $\tau_{0.55}$ bin spanned between 'C_i - N/2' and 'C_i + N/2'. If there were not enough observations near a certain $\tau_{0.55}$ value, we tried N=N_t/40. The spectral optical thickness for each bin was calculated by averaging the spectral optical thickness for the set of observations within the bin.

Figure 7 compares spectral dependence of the aerosol models with spectral dependence at selected AERONET sites, for selected indexed values of $\tau_{0.55}$. The MODIS LUT is calculated at four wavelengths (0.47, 0.55, 0.66 and 2.12 μm) channels, whereas AERONET spans four to eight bands between 0.34 and 1.02 μm (depending on which site). Though not contained in the lookup table, τ at 0.855 μm is also modeled for MODIS. Interpolation of AERONET to 2.12 μm was not performed because of the great distance from 1.02 μm. Different seasons (for AERONET) are represented by different line styles, whereas different $\tau_{0.55}$ indices (values) are color-coded. Because at some sites, the assumed aerosol type changes by season, spectral dependence for an additional model is plotted.

At Alta_Floresta (9°S, 56°W), the spectral dependence in the visible wavelengths agrees with either the neutral or absorbing models. At 0.855 μm, the AERONET spectral dependence varies as a function of season, which somewhat mirrors the differences in modeled spectral dependence. During the summer and fall, the AERONET dependence is slightly closer to the absorbing model than the neutral, and during the winter and spring, the neutral model provides a slightly better match.

At Capo_Verde (16°N, 22°W), although the neutral fine-dominated model is assumed all year, coarse (dust) is expected to dominate. Plotted for Capo_Verde is the AERONET spectral τ compared with the modeled dust. Even though we believe that we have improved the dust model from C004, the modeled spectral dependence is still too large to properly represent dust over Capo_Verde.

The non-absorbing model ($\omega_0 \sim 0.95$) shows remarkable match to observations at GSFC (39°N, 77°W). The only difference is seen during the winter and spring for the lowest τ value (0.25), where the particles are known to be larger (have less spectral dependence) than the rest of the year. Mongu (15°S, 23°E) is another site that is well represented by its assumed aerosol type (absorbing).

Beijing (39°N, 116°E) and Venise (45°N, 12°E) are interesting because dominant aerosol type is known to vary. Both sites are influenced by dust transport, so that the averaged AERONET spectral dependence should lie somewhere between the fine-dominated and coarse-dominated (dust) models. Due to plotting constrains, the coarse model (dust) spectral dependence is not plotted, but it is obvious that over Beijing the

aerosol is mixed neutral and dust, and more coarse-dominated during the winter and spring. Venise is less often in the path of dust (from Africa) but its averaged spectral dependence shows the addition of coarse aerosol not represented by a fine-dominated model.

7. Conclusion

Since 2000, MODIS has been capably retrieving aerosol properties over land. However, the long-term study of MODIS products led us to re-evaluate the assumed aerosol model physical and optical properties. We used the entire time series of almucantur-derived aerosol properties from all AERONET sites to compose a set of three fine-dominated (spherical) and one coarse-dominated (spheroid) aerosol optical models that seemed to best represent the global aerosol system. The fine-dominated aerosol types differed mainly by their values of ω_0, so se designated them as 'neutral' (ω_0~0.90), 'absorbing' (ω_0~0.85) and 'non-absorbing' (ω_0~0.95). We then created seasonal 1°x1° maps of designated aerosol type.

Phase functions for some of the models were nearly identical to the analogous models from C004 algorithm. One of the models (coarse) had substantially different phase function from the C004 due to the assumption of spheroids instead of spheres. Spectral dependence of τ of the models was compared with 'sun' retrieved observations from selected AERONET sites. Sites dominated by fine aerosol (e.g. GSFC and Mongu) were well represented by their assumed aerosol type. At Alta_Floresta, also dominated by fine aerosol, our seasonal choice of fine models (neutral versus absorbing) was correct. In a dust-dominated site such as Capo_Verde, our dust model has too much spectral dependence. Sites that are influenced by occasional dust episodes (e.g. Venise or Beijing) show spectral dependence lying between the fine and coarse –dominated models.

While the derivation of the new set of aerosol models is an interesting exercise in its own right, the real strength to the work will be its implementation within the new aerosol algorithm (Levy et al., 2006). Preliminary tests of the combination of updated aerosol models and new algorithm procedure is expected to improve the retrieved products for C005 (Levy et al., 2006).

However, we note that the MODIS evaluation is never complete. The AERONET data team has nearly completed revision of the sky products dataset. Reprocessing of this dataset may lead to updated aerosol models, especially for dust-dominated sites. We also plan to evaluate assumptions of ω_0, using independent datasets.

References

Ahmad, Z. and R. S. Fraser (1981). An Iterative Radiative Transfer Code For Ocean-Atmosphere Systems, *J. Atmos. Sci., 39*, 656-665.

Al-Saadi, J., J. Szykman, R. B. Pierce, C. Kittaka, D. Neil, D. A. Chu, L. Remer, L. Gumley, E. Prins, L. Weinstock, C. MacDonald, R. Wayland, F. Dimmick, and J. Fishman, (2005) Improving National Air Quality Forecasts with Satellite Aerosol Observations. *Bull. Am. Met. Soc., 86* (9), 1249-1261.

Bodhaine, B. A., N. B. Wood, et al. (1999), On Rayleigh optical depth calculations, *J. Atmos. Ocean. Tech., 16*(11), 1854-1861.

Chin, M., P. Ginoux, et al. (2002), Tropospheric aerosol optical thickness from the GOCART model and comparisons with satellite and Sun photometer measurements, *J. Atmos. Sci., 59*(3), 461-483.

Chu, D. A., Y. J. Kaufman, et al. (2002), Validation of MODIS aerosol optical depth retrieval over land, *Geophys, Res. Lett. 29*(12): art. no.-1617.

Chu, D. A., Y. J. Kaufman, G. Zibordi, J. D. Chern, J. Mao, C. Li, and B. N. Holben, (2003), Global monitoring of air pollution over land from EOS- Terra MODIS, *J. Geophys. Res., 108* (D21), 4661, doi: 10.1029/2002JD003179.

Dave, J. V. (1970), Intensity and Polarization of Radiation Emerging from a Plane-Parallel Atmosphere Containing Monodispersed Aerosols, *App. Optics, 9*(12): 2673-&.

Dubovik, O., B. Holben, et al. (2002a), Variability of absorption and optical properties of key aerosol types observed in worldwide locations, *J. Atmos. Sci. 59*(3), 590-608.

Dubovik, O., B. N. Holben, et al. (2002), Non-spherical aerosol retrieval method employing light scattering by spheroids, *Geophys, Res. Lett. 29*(10): art. no.-1415.

Dubovik, O. and M. D. King (2000), A flexible inversion algorithm for retrieval of aerosol optical properties from Sun and sky radiance measurements, *J. Geophys. Res, 105*(D16), 20673-20696.

Dubovik, O., A. Sinyuk, T. Lapyonok, B. N. Holben, M. Mishchenko, P. Yang, T. F. Eck, H. Volten, O. Munoz, B. Veihelmann, van der Zander, M Sorokin, and I. Slutsker, (2006) Application of light scattering by spheroids for accounting for

particle non-sphericity in remote sensing of desert dust, *J. Geophys. Res., 111*(D11208), doi: 10.1029/2005JD006619.

Eck, T. F., B. N. Holben, et al. (2005), Columnar aerosol optical properties at AERONET sites in central eastern Asia and aerosol transport to the tropical mid-Pacific, *J. Geophys. Res., 110*(D6).

Eck, T. F., B. N. Holben, et al. (1999), Wavelength dependence of the optical depth of biomass burning, urban, and desert dust aerosols, *J. Geophys. Res., 104*(D24), 31333-31349.

Evans, K.F. and G. L. Stephens, 1991, A New Polarized Atmospheric Radiative Transfer Model, *J. Quant. Spectrosc. Radiat. Transfer, 46*(5),413-423.

Fraser, R. H., Ferrare, R. A., Kaufman, Y. J., Mattoo, S. (1989). Algorithm for Atmospheric Corrections of Aircraft and Satellite Imagery. NASA Technical Memorandum 100751. Greenbelt, MD USA, NASA Goddard Space Flight Center.

Holben, B. N., T. F. Eck, et al. (1998), AERONET - A federated instrument network and data archive for aerosol characterization, *Remote. Sens. Environ., 66*(1), 1-16.

Hubanks, P. A. (2005), MODIS Atmosphere QA Plan for Collection 005. Greenbelt, MD USA, NASA Goddard Space Flight Center, 57 pages.

Ichoku, C., L. A. Remer, et al. (2003), MODIS observation of aerosols and estimation of aerosol radiative forcing over southern Africa during SAFARI 2000, *J. Geophys. Res., 108*(D13): art. no.-8499.

Ichoku, C., D. A. Chu, et al. (2002), A spatio-temporal approach for global validation and analysis of MODIS aerosol products, *Geophys. Res. Lett., 29*(12): art. no.-1616.

Ignatov, A., P. Minnis, N. Loeb, B. Wielicki, W. Miller, S. Sun-Mack, D. Tanré, L. Remer, I. Laszlo, and E. Geier (2005), Two MODIS Aerosol Products over Ocean on the Terra and Aqua CERES SSF Datasets, *J. Atm. Sci., 62*, 1008-1031.

Intergovernmental Panel on Climate Change (IPCC), 2001. Climate Change 2001: The Scientific Basis, J. T. Houghton, Y. Ding, D.J. Griggs, M. Noguer, P. J. van der Linden and D. Xiaosu (Eds.), Cambridge University Press, UK. pp 944.

Kaufman, Y. J., D. Tanré, et al. (1997), Operational remote sensing of tropospheric aerosol over land from EOS moderate resolution imaging spectroradiometer, *J.*

Geophys. Res., 102(D14),17051-17067.

Levy, R. C., L. A. Remer, et al. (2004), Effect of neglecting polarization on the MODIS aerosol retrieval over land, *IEEE Trans. Geosci. Remote. Sens., 42*(11), 2576-2583.

Levy, R. C., L. A. Remer, et al. (2005), Evaluation of the MODIS aerosol retrievals over ocean and land during CLAMS, *J. Atmos. Sci., 62*(4), 974-992.

Levy, R.C., L.A. Remer, S. Mattoo, E. Vermote, Y.J. Kaufman, (2006), A new algorithm for retrieving aerosol properties over land from MODIS spectral reflectance, submitted to JGR.

O'Neill, N. T., Eck, T. F., Smirnov, A., Holben, B. N. and Thulasiraman, S. (2003), Spectral discrimination of coarse and fine mode optical depth, *J Geophys. Res., 108*, doi:10.1029/2002JD002975.

O'Neill, N. T., Smirnov, A., Holben, B., and Thulasiraman, S. (2005), Spectral Deconvolution algorithm: Technical memo.

Omar, A. H., J. G. Won, et al. (2005), Development of global aerosol models using cluster analysis of Aerosol Robotic Network (AERONET) measurements, *J Geophys. Res., 110*(D10).

Remer, L. A. and Y. J. Kaufman (1998), Dynamic aerosol model: Urban/industrial aerosol, *J Geophys. Res., 103*(D12): 13859-13871.

Remer, L. A., Y. J. Kaufman, et al. (2005), The MODIS aerosol algorithm, products, and validation *J. Atmos. Sci., 62*(4), 947-973.

U.S. Government Printing Office, (1976), U.S. Standard Atmosphere, Washington, D.C.

Vermote, E. F., D. Tanré, et al. (1997), Second Simulation of the Satellite Signal in the Solar Spectrum, 6S: An overview *IEEE Trans. Geosci. Remote Sens., 35*(3), 675-686.

Wiscombe, W. J. (1981). "Improved Mie scattering algorithms." *Appl. Opt. 19*, 1505-1509.

Yu, H., Y. J. Kaufman, M. Chin, G. Feingold, L. Remer, T. Anderson, Y. Balkanski, N. Bellouin, O. Boucher, S. Christopher, P. DeCola, R. Kahn, D. Koch, N. Loeb, M. S. Reddy, M. Schulz, T. Takemura, and M. Zhou (2006), A review of

measurement-based assessments of aerosol direct radiative effect and forcing, *Atmos. Chem . Phys.*, *6*, 613-666.

Appendix 1: Derivation of Extinction, Scattering and Mass Coefficients

The following equations lead to derivation of Mass Concentration in units of (μg per cm^2). In these equations: $dN/d\ln r$ is the number size distribution with r denoting radius (in μm). For a lognormal mode, r_g is the geometric mean radius, σ is $\ln\sigma_g$ representing the standard deviation of the radius, and N_0 is the number of particles per cross section of the atmospheric column (i.e. the amplitude of the lognormal size distribution). In our case, we assume that the distribution is normalized, so that N_0=1.

The number N is related to the volume V and area A distributions by:

$$\frac{dN}{d\ln r} = \frac{3}{4}\pi r^{-3}\frac{dV}{d\ln r} = \pi r^{-2}\frac{dA}{d\ln r}.$$

N_0, V_0, and A_0 are the amplitudes of the corresponding distributions, i.e.

$$V_0 = \int_0^\infty \frac{dV}{d\ln r}d\ln r \quad N_0 = \int_0^\infty \frac{dN}{d\ln r}d\ln r \quad A_0 = \int_0^\infty \frac{dA}{d\ln r}d\ln r.$$

For a single lognormal mode defined by:

$$\frac{dN}{d\ln r} = \frac{1}{r}\frac{N_0}{\sigma\sqrt{2\pi}}\exp\left(-\frac{\ln(r/r_g)^2}{2\sigma^2}\right)$$

and

$$N_0 = V_0\frac{3}{4}\pi r_g^{-3}\exp\left(-\frac{9}{2}\sigma^2\right),$$

the Moments of order k, M^k are defined as

$$M^k = \int_0^\infty r^k\frac{dN}{d\ln r}d\ln r = (r_g)^k\exp(0.5k^2\sigma^2).$$

The effective radius r_{eff} in (μm] is defined by the moments, i.e.

$$r_{eff} = \frac{M^3}{M^2} = \frac{\int_0^\infty r^3 \frac{dN}{d\ln r} d\ln r}{\int_0^\infty r^2 \frac{dN}{d\ln r} d\ln r} = \frac{3}{4}\frac{V_0}{A_0} = r_g \exp(\frac{5}{2}\sigma^2)$$

The extinction coefficient, β_{ext} is related to the extinction efficiency Q_{ext} through the area distribution, and is specific to each mode

$$Q_{ext} = \frac{\beta_{ext}}{\int_0^\infty \pi r^2 \frac{dN}{d\ln r} d\ln r}$$

These parameters are calculated via Mie code (MIEV, (Wiscombe, 1980)). Note that the scattering coefficient β_{sca} and efficiency Q_{sca} are related the same way. The mass extinction coefficient B_{ext} is in units of (area per mass) and depends on the extinction efficiency and the particle density ρ (assumed to be 1 g per cm^3), such that

$$B_{ext} = \frac{3Q_{ext}}{4\rho r_{eff}}.$$

(Chin et al., 2002). For a single lognormal mode,

$$B_{ext} = \frac{3Q_{ext}}{4\rho r_{eff}} = \frac{3}{4}\frac{Q_{ext}}{\rho}\frac{A_0}{(3/4)V_0} = \frac{Q_{ext}}{\rho}\frac{A_0}{V_0} = \frac{\beta_{ext}}{\rho V_0} = \frac{3\beta_{ext}}{4\rho\pi r_g^3 \exp(4.5\sigma^2)}.$$

However our aerosol models are sums of multiple modes, so that the area and volume distributions must take into account the contributions of each mode. If there are two modes, (i.e. modes 1 and 2), r_{eff} must be calculated this way:

$$r_{eff} = \frac{\int_0^\infty r^3 \frac{(dN_1 + dN_2)}{d\ln r} d\ln r}{\int_0^\infty r^2 \frac{(dN_1 + dN_2)}{d\ln r} d\ln r}$$

Similar modifications are made when calculating Q and thus B.

We can define the Mass Concentration Coefficient M_c, as the inverse of B, such that

$$M_c = \frac{1}{B}.$$

The columnar mass concentration, M (mass per area) can then be defined as

$$M = \tau M_c = \frac{\tau}{B}$$

TABLE 1: OPTICAL PROPERTIES OF THE AEROSOL MODELS USED FOR THE V5.2 OVER-LAND LOOKUP TABLE

Model	Mode	r_v (μm)	σ	V_0 ($\mu m^3/\mu m^2$)	Refractive Index: k	SSA/g (0.47/0.55/0.66/2.1μ M) for $\tau_{0.55} = 0.5$
Continental						0.90/0.89/0.88/0.67 0.64/0.63/0.63/0.79
	Soluable	0.176	1.09	3.05	1.53-0.005i; 0.47 μm 1.53-0.006i; 0.55 μm 1.53-0.006i; 0.66 μm 1.42-0.01i; 2.12 μm	
	Dust	17.6	1.09	7.364	1.53-0.008i; 0.47 μm 1.53-0.008i; 0.55 μm 1.53-0.008i; 0.66 μm 1.22-0.009i; 2.12 μm	
	Soot	0.050	0.693	0.105	1.75-0.45i; 0.47 μm 1.75-0.44i; 0.55 μm 1.75-0.43i; 0.66 μm 1.81-0.50i; 2.12 μm	
Neutral/ Generic						0.93/0.92/0.91/0.87 0.68/0.65/0.61/0.68
	Accum	$0.0203\tau + 0.145$	$0.1365\tau + 0.3738$	$0.1642\,\tau^{0.7747}$	$1.43 - (-0.002\tau+0.008)i$	
	Coarse	$0.3364\tau + 3.101$	$0.098\tau + 0.7292$	$0.1482\,\tau^{0.6846}$	$1.43 - (-0.002\tau+0.008)i$	
Non-absorb/ Urban-Ind						0.95/0.95/0.94/0.90 0.71/0.68/0.65/0.64
	Accum	$0.0434\tau + 0.1604$	$0.1529\tau + 0.3642$	$0.1718\,\tau^{0.8213}$	$1.42 - (-0.0015\tau+0.007)i$	
	Coarse	$0.1411\tau + 3.3252$	$0.1638\tau + 0.7595$	$0.0934\,\tau^{0.6394}$	$1.42 - (-0.0015\tau+0.007)i$	
Absorbing/ Heavy Smoke						0.88/0.87/0.85/0.70 0.64/0.60/0.56/0.64
	Accum	$0.0096\tau + 0.1335$	$0.0794\tau + 0.3834$	$0.1748\,\tau^{0.8914}$	$1.51 - 0.02i$	
	Coarse	$0.9489\tau + 3.4479$	$0.0409\tau + 0.7433$	$0.1043\,\tau^{0.6824}$	$1.51 - 0.02i$	
Spheroid/ Dust						0.94/0.95/0.96/0.98 0.71/0.70/0.69/0.71
	Accum	$0.1416\,\tau^{-0.0519}$	$0.7561\,\tau^{0.148}$	$0.0871\,\tau^{1.026}$	$1.48\tau^{-0.021} - (0.0025\,\tau^{0.132})i$; 0.47 μm $1.48\tau^{-0.021} - 0.002i$; 0.55 μm $1.48\tau^{-0.021} - (0.0018\,\tau^{-0.08})i$; 0.66 μm $1.46\tau^{-0.040} - (0.0018\,\tau^{-0.30})i$; 2.12 μm	
	Coarse	2.2	$0.554\,\tau^{-0.0519}$	$0.6786\,\tau^{1.0569}$	$1.48\tau^{-0.021} - (0.0025\,\tau^{0.132})i$; 0.47 μm $1.48\tau^{-0.021} - 0.002i$; 0.55 μm $1.48\tau^{-0.021} - (0.0018\,\tau^{-0.08})i$; 0.66 μm $1.46\tau^{-0.040} - (0.0018\,\tau^{-0.30})i$; 2.12 μm	

Listed for each model are the individual lognormal modes, and the final SSA at different wavelengths. Listed for each mode are the mean radius r_v, standard deviation σ of the volume distribution, and total volume of the mode, V_0. The complex refractive index is assumed for all wavelengths (0.47, 0.55. 0.66 and 2.1 μm), unless otherwise noted. The Absorbing and Neutral model parameters (r_v, σ and k) are defined for $\tau \leq 2.0$; for $\tau > 2.0$, we assume $\tau = 2.0$. Likewise, the Non-absorbing and Spheroid model parameters are defined for $\tau \leq 1.0$. V_0 (for all models) is defined for all τ.

TABLE 2: CHARACTERISTICS OF MODIS CHANNELS USED IN THE AEROSOL RETRIEVAL

Band #	Bandwidth (μm)	Weighted Central Wavelength (μm)	Resolution (m)	Rayleigh optical depth
1	0.620 - 0.670	0.646	250	0.0520
2	0.841 - 0.876	0.855	250	0.0165
3	0.459 - 0.479	0.466	500	0.1948
4	0.545 - 0.565	0.553	500	0.0963
5	1.230 – 1.250	1.243	500	0.0037
6	1.628 – 1.652	1.632	500	0.0012
7	2.105 – 2.155	2.119	500	0.0004

Notes: Band #26 (1.38 μm channel) is used for cirrus correction; NeΔρ corresponds to the sun at zenith ($\theta = 0°$)

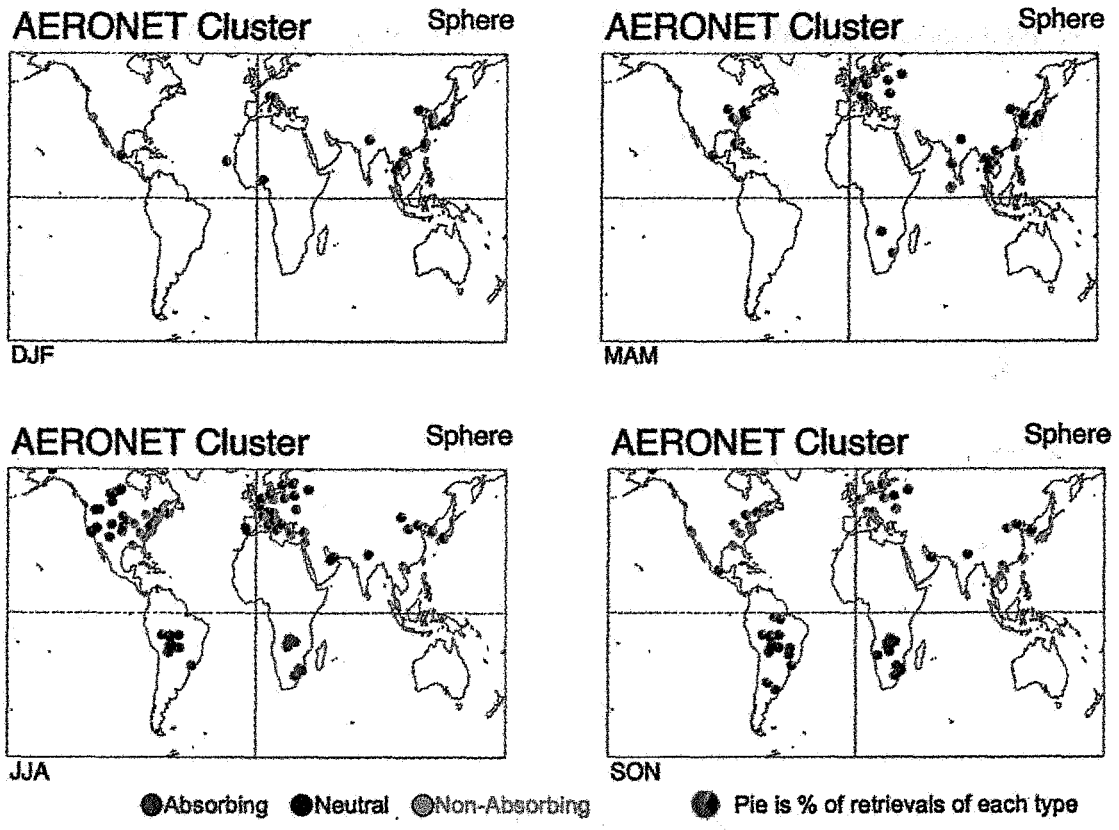

Figure 1: Percentage (pie charts) of spherical aerosol model type retrieved at each AERONET site per season. Colors represent absorbing (ω_0~0.85), neutral (ω_0~0.90) and non-absorbing (ω_0~0.95), respectively.

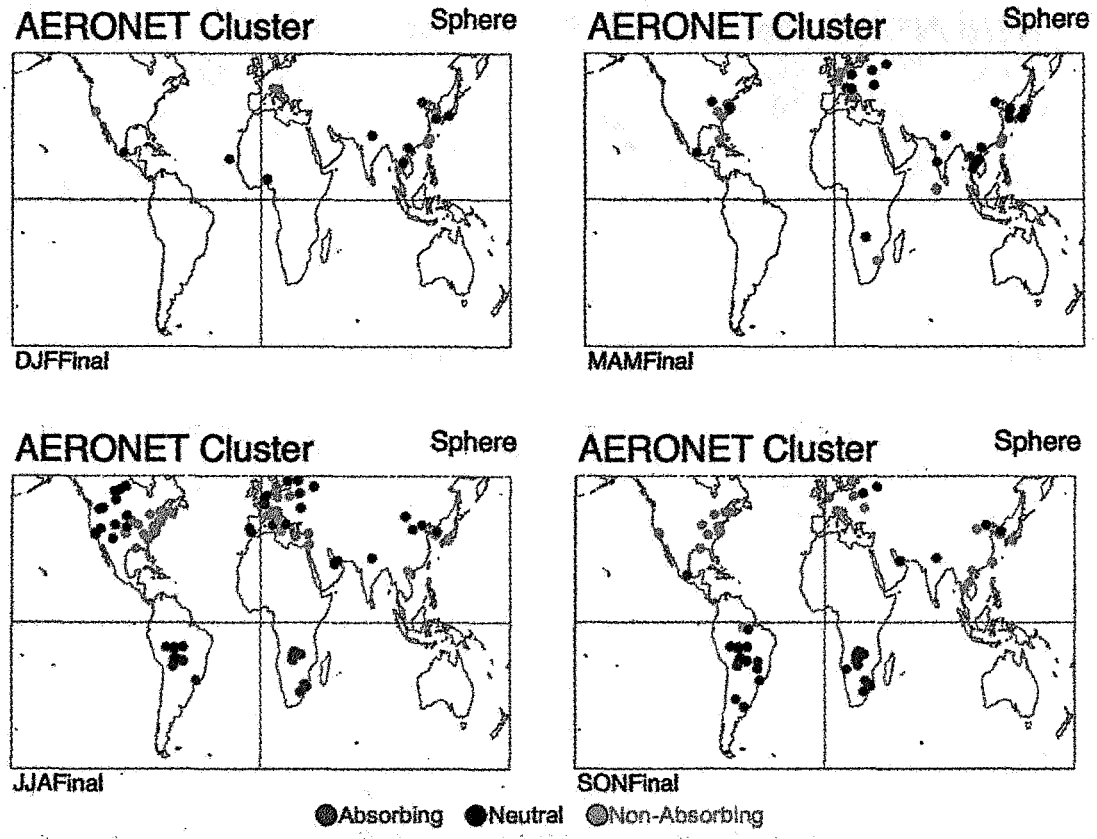

Figure 2: Final spherical aerosol model type designated at each AERONET site per season. Colors represent absorbing (ω_0~0.85), neutral (ω_0~0.90) and non-absorbing (ω_0~0.95), respectively.

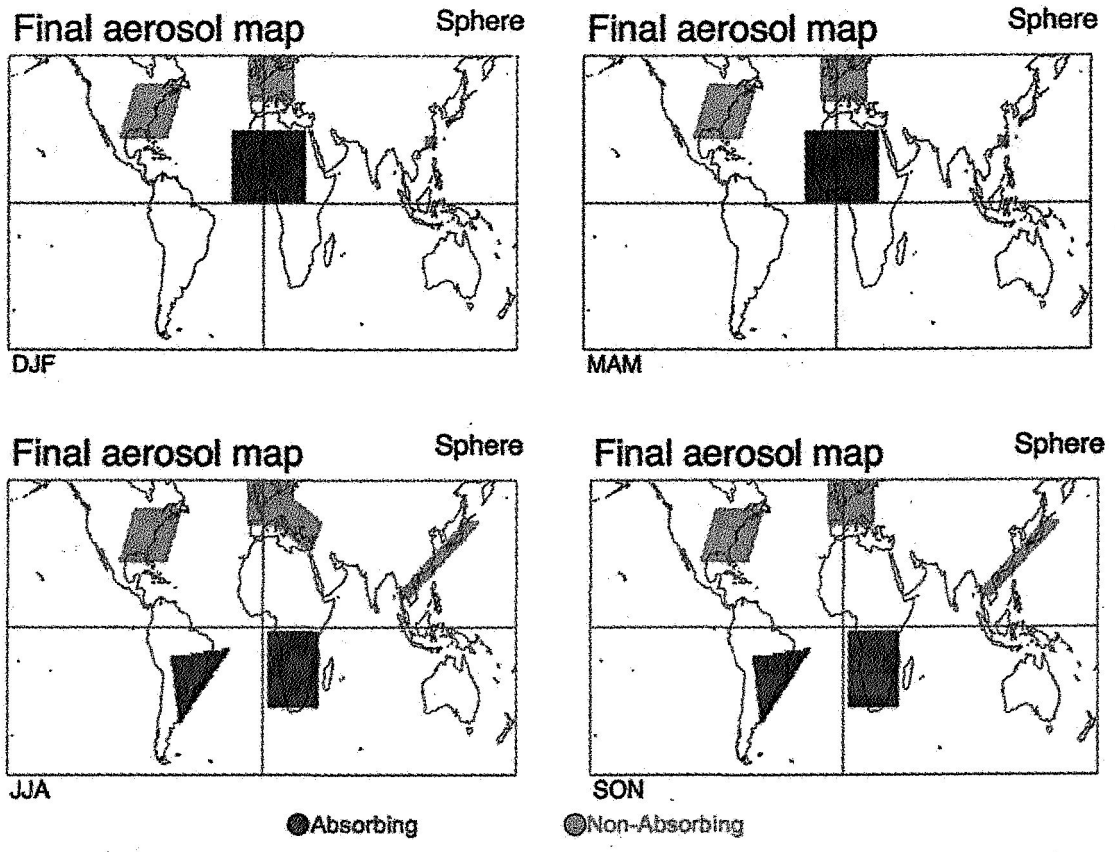

Figure 3: Final spherical aerosol model type designated at 1° x 1° gridbox per season. Red and green represent absorbing (ω_0~0.85) or non-absorbing (ω_0~0.95) models, respectively. Neutral (ω_0~0.90) is assumed everywhere else.

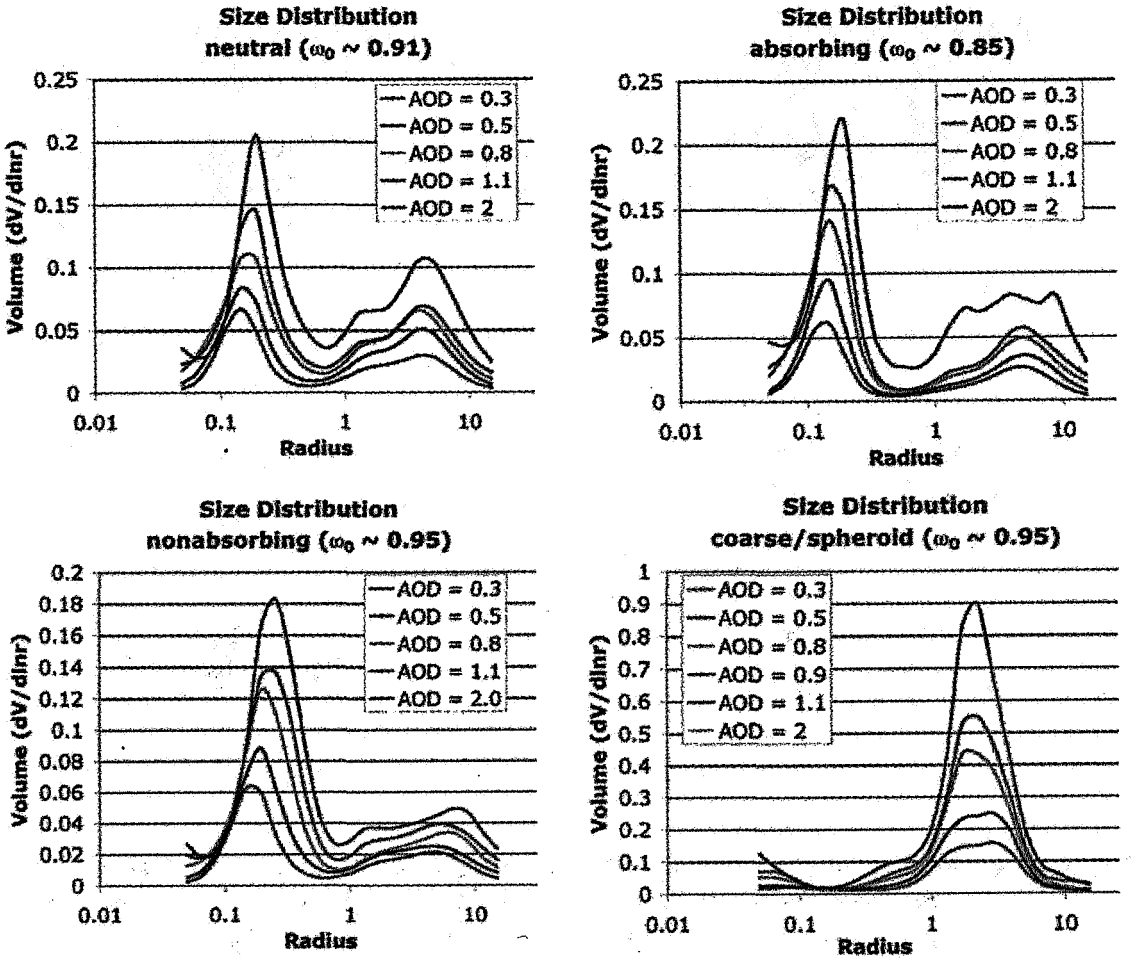

Figure 4: Aerosol size distribution as a function of τ (AOD) bin for the three spherical (neutral, absorbing and non-absorbing) and spheroid (dust) models identified by clustering of AERONET.

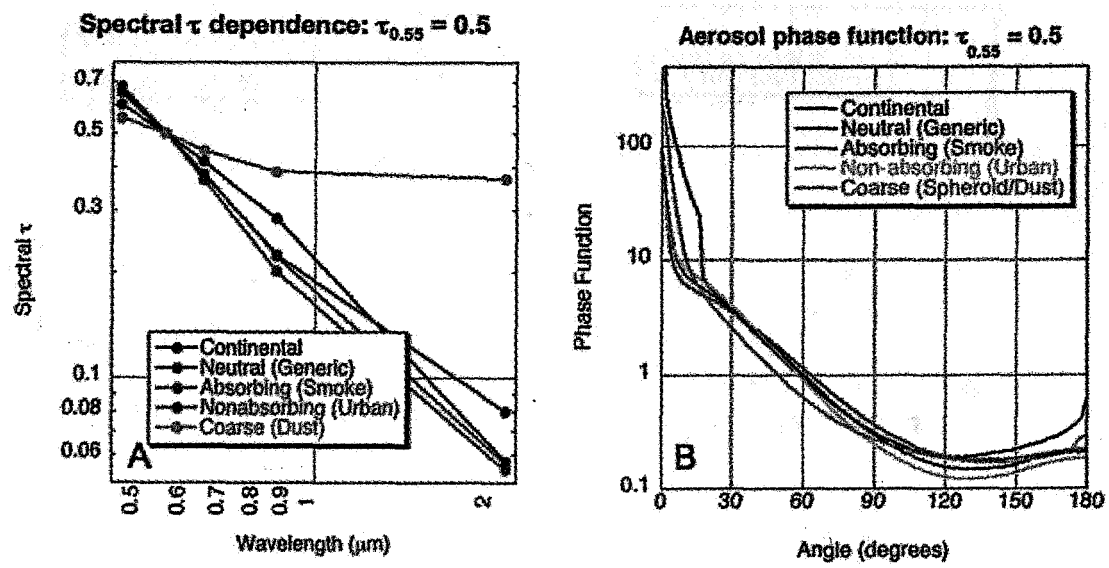

Figure 5: Spectral τ dependence (A) and phase function at 0.55 μm (B) for the 5 aerosol models in of the V5.2 LUT. For both plots, $\tau_{0.55}$ = 0.5.

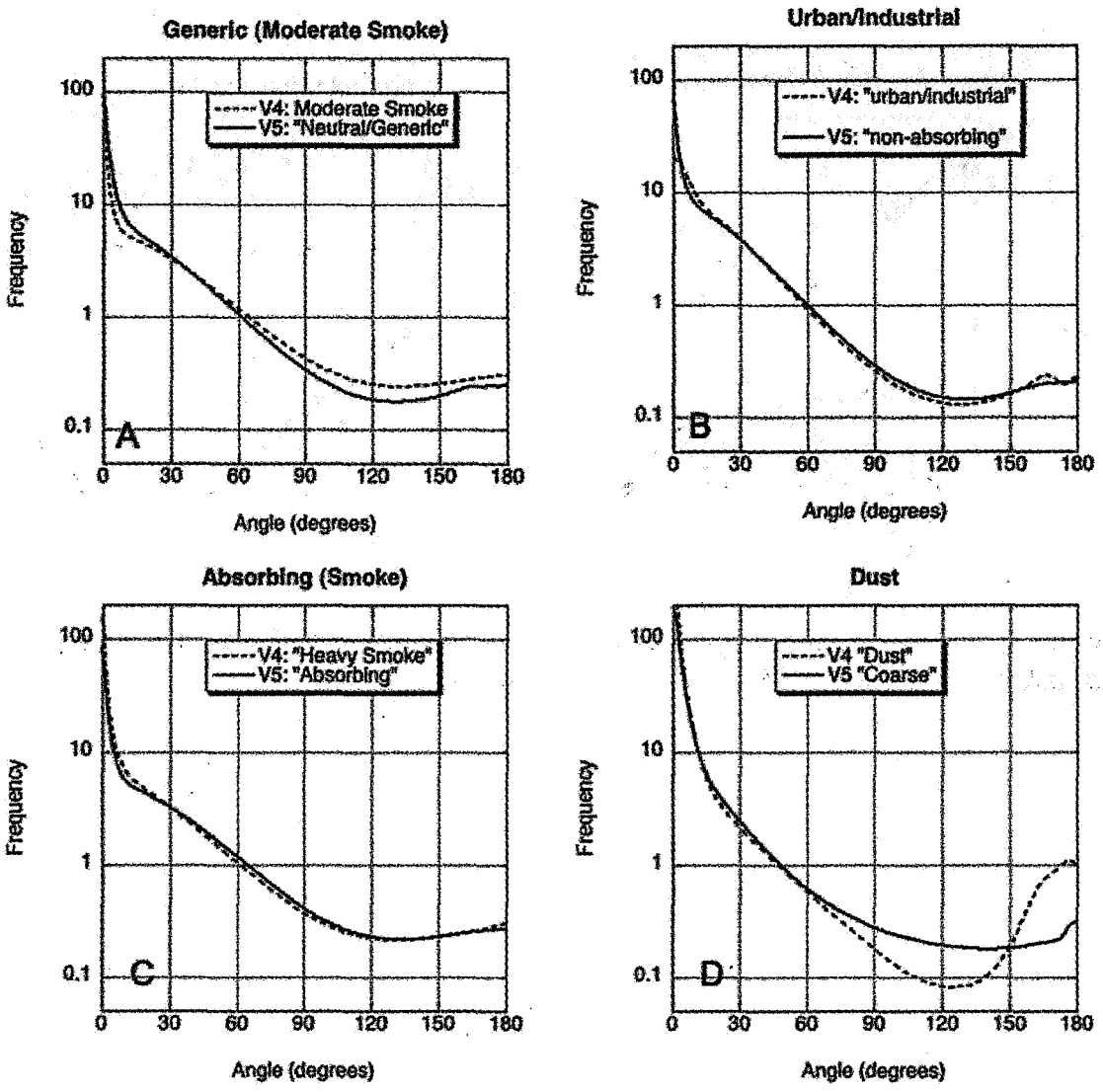

Figure 6: Comparison of phase function (at 0.55 μm) between V5 (solid curves) and analogous V4 (dotted curves) aerosol models. Models are neutral (A), nonabsorbing (B), absorbing (C) and dust (D). For all plots, $\tau_{0.55} = 0.5$.

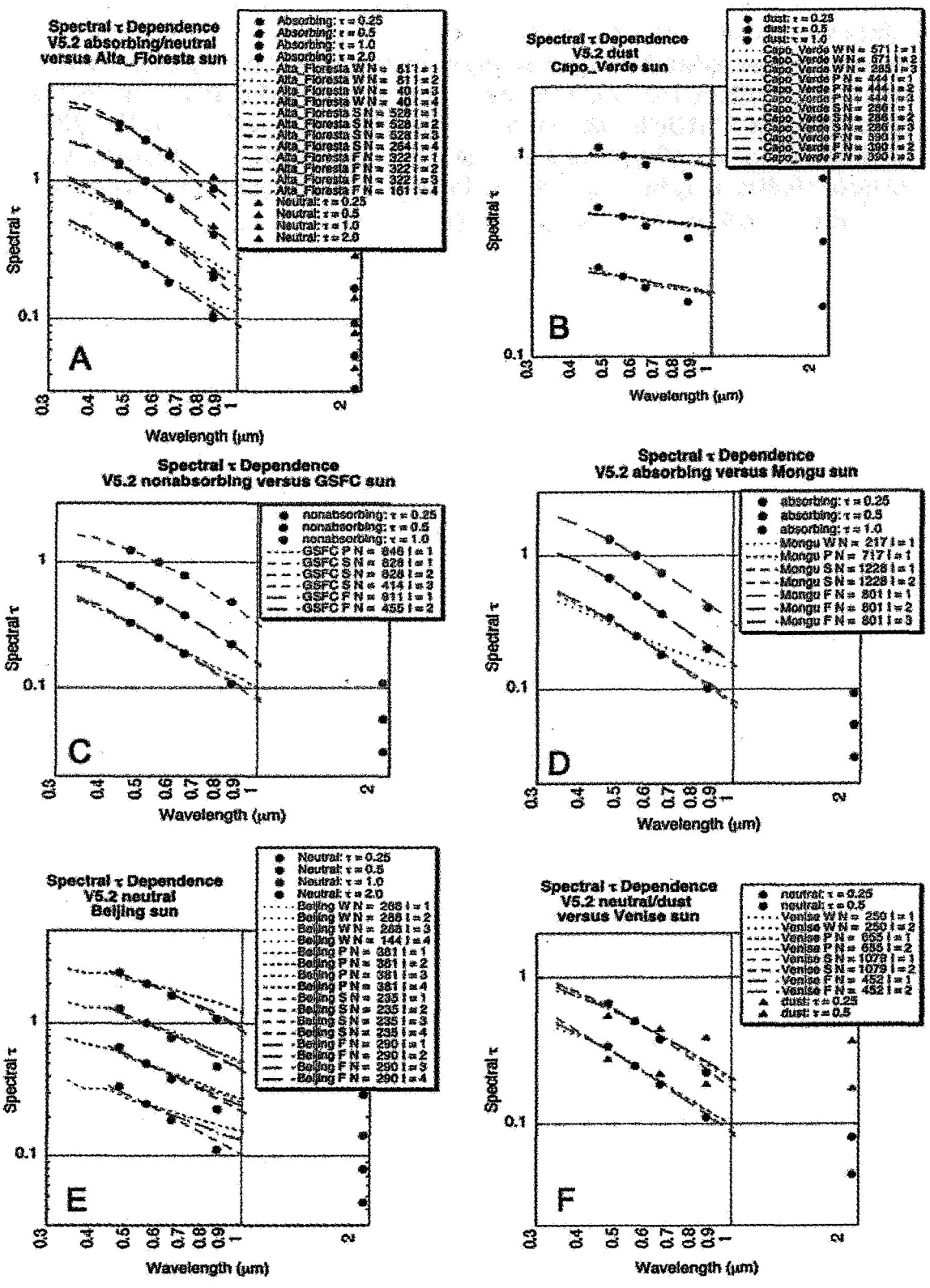

Figure 7: Comparison of spectral τ between V5 models (filled shapes) and averages of AERONET 'sun' measurements (dotted curves) at selected sites and seasons. The colors represent discrete (Indexed=I) values of $\tau_{0.55}$, such that green=$\tau_{0.55}$=0.25=I=1,

blue= $\tau_{0.55}$=0.5=I=2, red=$\tau_{0.55}$=1.0=I=3 and black=$\tau_{0.55}$=2.0=I=4. Different curve types represent AERONET data during a season (dot = DJF (W), short dash = MAM (P), medium dash = JJA (S) and long dash = SON (F)). In the legend, 'N' is the number of AERONET observations contained within each curve. Note that for each site, spectral τ of more than one aerosol model and/or fewer than all seasons and all τ indices may be plotted. Sites plotted are Alta_Floresta (A), Capo_Verde (B), GSFC (C), Mongu (D), Beijing (E) and Venise (F).